Kinetic Characterization of the Second Step of Group II Intron Splicing: Role of Metal Ions and the Cleavage Site 2′-OH in Catalysis†

Peter M. Gordon,‡ Erik J. Sontheimer,‡,§ and Joseph A. Piccirilli*,‡,||

Howard Hughes Medical Institute, Department of Biochemistry and Molecular Biology, and Department of Chemistry, The University of Chicago, 5841 South Maryland Avenue, MC1028, Chicago, Illinois 60637

Received May 12, 2000; Revised Manuscript Received August 9, 2000

ABSTRACT: The ai5γ group II intron from yeast excises itself from precursor transcripts in the absence of proteins. When a shortened form of the intron containing all but the 3′-terminal six nucleotides is incubated with an exon 1 oligonucleotide and a 3′ splice site oligonucleotide, a nucleotidyl transfer reaction occurs that mimics the second step of splicing. As this tripartite reaction provides a means to identify important functional groups in 3′ splice site recognition and catalysis, we establish here a minimal kinetic framework and demonstrate that the chemical step is rate-limiting. We use this framework to characterize the metal ion specificity switch observed previously upon sulfur substitution of the 3′-oxygen leaving group and to elucidate by atomic mutagenesis the role of the neighboring 2′-OH in catalysis. The results suggest that both the 3′-oxygen leaving group and the neighboring 2′-OH are important ligands for metal ions in the transition state but not in the ground state and that the 2′-OH may play an additional role in transition state stabilization by donating a hydrogen bond. Metal specificity switch experiments combined with quantitative analysis show that the Mn^{2+} that interacts with the leaving group binds to the ribozyme with the same affinity as the metal ion that interacts with the neighboring 2′-OH, raising the possibility that a single metal ion mediates interactions with the 2′- and 3′-oxygen atoms at the 3′ splice site.

Group II introns are found in bacteria and in the organelles of plants, fungi, and algae (*1*). Some group II introns are autocatalytic, excising themselves from precursor RNAs in the absence of any protein factors. Self-splicing requires folding of the RNA into an active structure that catalyzes two sequential phosphotransesterification reactions to produce a free intron and ligated exons (for review, see ref *2*). In the first reaction, a water molecule or the 2′-hydroxyl group of a conserved intron adenosine residue attacks the phosphodiester bond at the 5′ splice site and generates an intron/3′ exon intermediate and a free 5′ exon (Figure 1A). In the second reaction, the free 3′-hydroxyl group of the 5′ exon attacks the phosphodiester bond at the 3′ splice site to produce ligated exons and an excised intron.

The chemical pathway by which the group II introns are spliced is the same as that by which nuclear pre-mRNAs are spliced by the spliceosome, a large ribonucleoprotein complex that catalyzes the excision of the vast majority of nuclear introns (*2*, *3*). This observation and other biochemical and structural similarities between the group II introns and the spliceosome have fueled speculation that the two splicing machineries share a common molecular ancestor and that the spliceosome may be an RNA catalyst (*2*, *4*). A comparison of group II and spliceosomal catalytic mechanisms can provide valuable insight into possible evolutionary relationships (*5*) as catalytic features are among the molecular traits of enzymes that are believed to be most highly conserved during evolution (*6*). Thus, understanding the similarities and differences between these two systems is important, not only for our understanding of contemporary gene expression but also because it can reveal clues about the origin and evolution of gene organization. Furthermore, a mechanistic comparison of the group II intron with other large ribozymes (self-splicing group I introns, RNase P) may provide additional insight into the repertoire of catalytic strategies available to RNA. However, the catalytic mechanisms employed by group II introns and the spliceosome during each step of splicing remain largely unknown. For both steps of splicing, phosphotransesterification reactions occur via direct in-line S_N2 nucleophilic attack (*7*, *8*), and a divalent metal ion stabilizes the 3′-oxyanion leaving group (*5*, *9*, *10*).

To examine mechanisms of ribozyme catalysis, it is often necessary to develop assays or reaction conditions that isolate a single step of splicing and that monitor the chemical step of the reaction. The development of such assays, however, is hampered by difficulties in separating divalent metal ion dependent folding from catalytic events under *cis*-splicing conditions, in which the intron (ribozyme) is covalently linked to the flanking exons (substrates). This problem is circumvented in several group II intron multipartite (*trans*) assays that divide the splicing construct into a substrate portion and a ribozyme portion that can be independently folded into a catalytically active structure before the addition of substrate.

† This work is supported by the Howard Hughes Medical Institute.

* To whom correspondence should be addressed. Phone: 773-702-9312. Fax: 773-702-0271. E-mail: jpicciri@midway.uchicago.edu.

‡ Department of Biochemistry and Molecular Biology.

§ Current address: Department of Biochemistry, Molecular Biology, and Cell Biology, Northwestern University, 4-120 Hogan Hall, 2153 North Campus Drive, Evanston, IL 60208-3500.

|| Department of Chemistry.

10.1021/bi001089o CCC: $19.00
Published on Web 09/30/2000

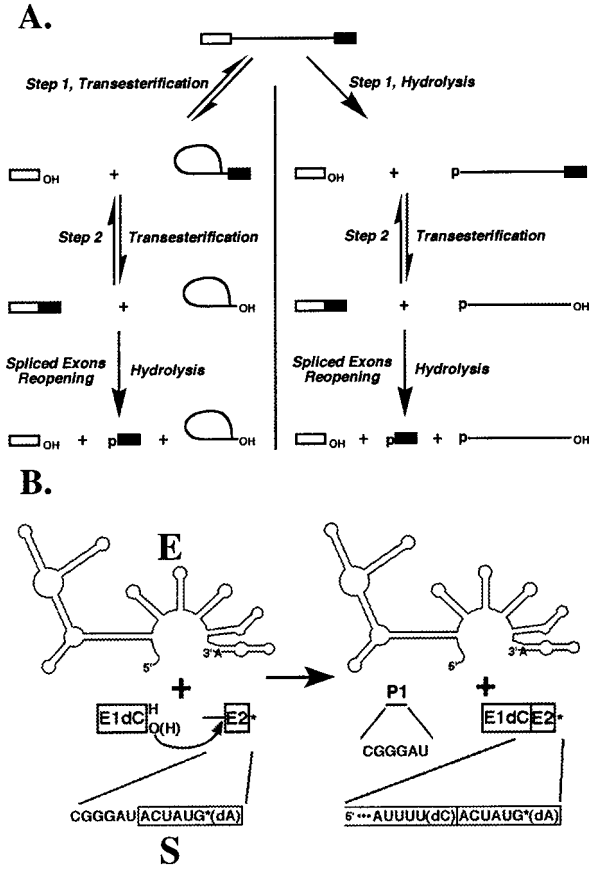

FIGURE 1: (A) Schematic representation of the two pathways of group II intron self-splicing (*2*). The two pathways differ in the identity of the nucleophile in the first step of splicing. In the transesterification (branching) pathway the nucleophile is the 2′-OH of a conserved intron adenosine residue, while in the hydrolytic pathway the nucleophile is a water or hydroxide. (B) Tripartite reaction for the second step of splicing. A truncated form of the ai5γ group II intron [containing nucleotides 1−881 and lacking the last six nucleotides (882−887)] catalyzes the attack of an exon 1 oligonucleotide (E1) on a 13-nucleotide 3′ splice site substrate oligoribonucleotide. The 18-nucleotide E1 oligonucleotide used in this work (E1dC) contained a 3′-terminal 2′-deoxycytidine residue.

For the first step of group II self-splicing, there are *trans*-splicing systems that monitor the hydrolytic (*11*), branching (*12*−*14*), and reverse branching pathways (*15*). For the second step of splicing, addition of a free 5′ exon oligonucleotide to the linear intron/3′ exon (*16*−*19*) or the lariat intron/3′ exon (*15*) reconstitutes the second step of splicing through the hydrolytic or branching pathway, respectively. Use of a 5′ exon oligonucleotide containing a 2′-deoxycytidine at the 3′-terminus appears to render the chemical step rate-limiting for both reactions, although the catalytic rate is approximately 1000-fold faster in the branching pathway (*15*, *19*; see Discussion).

Despite this, detailed mechanistic studies on the second step of splicing are challenging. Atomic level modifications near the splice site that facilitate determination of the roles of specific functional groups require RNA ligation reactions that are often inefficient. Thus it can be exceedingly difficult to generate modified substrate for analysis of structure−function relationships. Moore and co-workers (Brandeis University) developed a tripartite assay for the second step of splicing in which a 3′ splice site oligonucleotide is added to a 5′ exon oligonucleotide and a ribozyme containing all but the six 3′-terminal nucleotides of the intron (Figure 1B). The small size of the 3′ splice site oligonucleotide (12-mer) allows for efficient chemical synthesis of modified substrates. In previous work, for example, we replaced the 3′-oxygen leaving group at the splice site with sulfur and used the modified substrate to uncover a metal ion/leaving group interaction that was masked by rate-limiting conformational changes during *cis*-splicing (*5*).

Herein, we report the basic kinetic characterization of the tripartite assay and establish a framework for exploring the energetic contributions of functional groups and metal ions to catalysis. Using metal specificity switch experiments together with recently developed quantitative approaches (*20*), we obtained thermodynamic signatures for specific metal ions in catalysis. The results provide evidence that both the 3′-oxygen leaving group and the neighboring 2′-OH serve as metal ion ligands in the transition state, possibly chelating to a single metal ion.

MATERIALS AND METHODS

Materials. Ribozyme, consisting of nucleotides 1−881 of the ai5γ group II intron from the mitochondrial gene COX1 of *Saccharomyces cerevisiae*, was prepared by in vitro transcription as described previously (*5*). Oligonucleotides were synthesized on a Millipore solid-phase DNA/RNA synthesizer. 3′-*S*-Phosphoramidites were synthesized and coupled as described by Sun et al. (*21*). Oligonucleotides for inhibition studies and phosphorothioate-containing oligonucleotides were supplied by Dharmacon Research. E1dC and E1rC (*19*) were purified by denaturing gel electrophoresis. Oligonucleotide substrates were 3′-end-labeled with [α-^{32}P]-3′-deoxyadenosine triphosphate (New England Nuclear) and yeast poly(A) polymerase according to manufacturer's instructions (Amersham Pharmacia).

Separation and Assignment of Configuration of Phosphorothioate Oligoribonucleotides. The diastereomers that arise from sulfur substitution at the scissile phosphate were separated by reverse-phase HPLC on a Beckman ODS Ultrasphere C_{18} reverse-phase column (10 × 250 mM) using a linear gradient of 0−18% solvent B over 40 min: solvent A was 0.1 M ammonium acetate, and solvent B was 100% acetonitrile. The configuration of each diastereomer was assigned by nuclease digestion, essentially as described by Slim et al. (*22*). In separate reactions, the purified diastereomers (∼0.5 nmol) were digested with snake venom phosphodiesterase (1 μg, Pharmacia Biotech) and nuclease P1 (1 μg, Pharmacia Biotech) in the presence of calf intestinal alkaline phosphatase (40 units, Pharmacia Biotech). To generate standards for comparison, the diastereomers of a phosphorothioate-containing dinucleotide [Up(s)A] were also HPLC-purified and digested with nucleases. Nuclease was removed with a microcon-10 spin column (Millipore), and nucleoside and dinucleotide products were analyzed by reverse-phase HPLC on a Beckman ODS Ultrasphere C_{18} reverse-phase column (4.6 × 250 mM) using a linear gradient of 0−30% solvent B over 50 min: solvent A was 0.01 M ammonium acetate, and solvent B was 100% acetonitrile.

General Kinetic Methods. Reactions were performed and analyzed essentially as described (*5*). For single turnover reactions the ribozyme was in excess of the radioactively labeled substrate. Reactions were performed at 42 °C and

contained ribozyme, E1dC (or E1rC), 0.5 M $(NH_4)_2SO_4$, 40 mM buffer at the pH indicated (sodium acetate, pH 5−6; NaMES,[1] pH 6−6.5; NaMOPS, pH 6.5−7.5), 100 mM $MgCl_2$, and $MnCl_2$ as specified. All tripartite reactions were performed with E1dC in excess of ribozyme and at a concentration at least 15-fold greater than its K_d (low nM; *23*). We also measured the rate of exon ligation as a function of E1dC concentration and confirmed that under our assay conditions E1dC was saturating (data not shown). Divalent metal ion chlorides were >99.99% pure (Aldrich). Before reaction, all components except for substrate and $MnCl_2$ were preincubated at 75 °C for 2 min followed by 42 °C for 90 min. Other renaturation and incubation protocols were tested, but they gave less reproducible data and often resulted in a considerable lag phase in the reaction course. Reactions were initiated by the addition of substrate, and six to eight 1 μL aliquots of reaction mixture were removed at specified times and quenched by the addition of 3 μL of stop solution (8 M urea/0.5× TBE/50 mM EDTA/0.04% xylene cyanol/0.01% bromophenol blue). Substrates and products were fractionated by denaturing 20% polyacrylamide gel electrophoresis, and their ratio at each time point was quantitated with a Molecular Dynamics phosphorimager.

Multiple turnover reactions, with substrate in excess of ribozyme, contained all of the reaction components described above. However, reactions were initiated by the addition of trace radioactively labeled substrate (1 nM) and unlabeled substrate as specified. Similar to multiple turnover reactions, competition experiments were initiated by the addition of trace radiolabeled S_{WT} and unlabeled inhibitor as specified.

Reactions were generally monitored for more than three half-lives. Reaction rates were calculated from first-order fits to the data with end points >98% (KaleidaGraph, Synergy Software, Reading, PA). For slow reactions, the observed rate constants were calculated from initial rates. Kinetic parameters varied no more than 2−3-fold when determined on separate occasions.

Determination of the pK_a of the 2′-Amino Group in the E^{E1dC}·$S_{2'N}$ Ternary Complex. The different reactivities of the 2′-NH_2 and 2′-NH_3^+ substrates in Mn^{2+} provide a means to detect the deprotonation of the 2′-NH_3^+ group and to determine its pK_a. The pH dependencies for the reactions of S_{WT} and $S_{2'N}$ were determined with saturating ribozyme in the presence of 100 mM Mg^{2+} or 100 mM Mg^{2+}/10 mM Mn^{2+}. The reactivity of $S_{2'N}$ in Mn^{2+} relative to the rate in Mg^{2+} was plotted as a function of pH, and the data were fit to eq 1, which was derived from Scheme 1.

Scheme 1

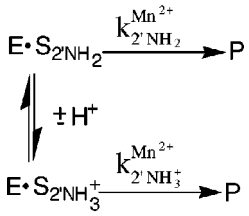

$$k_{obs}^{rel} = \frac{\frac{k_{S_{2'NH_2}}^{Mn^{2+}}}{k_{S_{WT}}^{Mn^{2+}}}}{1+\frac{[H^+]}{K_a}} + \frac{\frac{k_{S_{2'NH_3^+}}^{Mn^{2+}}}{k_{S_{WT}}^{Mn^{2+}}}}{1+\frac{K_a}{[H^+]}} \quad (1)$$

Cis-Splicing Reactions. A *cis*-splicing construct consisting of the ai5γ group II intron and flanking exons from the mitochondrial COX1 gene from *S. cerevisiae* was transcribed with T7 RNA polymerase from a *Hin*dIII linearized pJD20 plasmid (*17*). *Cis*-splicing reactions were performed as described (*24*) and contained trace radiolabeled substrate, 0.5 M $(NH_4)_2SO_4$, 40 mM MOPS (pH 7.5), and 100 mM $MgCl_2$. The rate of *cis*-splicing via the hydrolytic pathway was calculated according to the method of Daniels et al. (*24*).

RESULTS

General Kinetic Characterization of the Tripartite Exon Ligation Assay. The tripartite reaction mimics the second step of ai5γ group II intron self-splicing. In this assay a 3′ splice site oligonucleotide (S) is incubated with a 5′ exon oligonucleotide (E1) and the ribozyme (E, the linear intron). Numerous tripartite combinations are possible, depending on the site at which the 3′ splice site oligonucleotide is detached from the intron. In the reaction studied herein, the 3′ splice site oligonucleotide contains the last six nucleotides of the intron and the first six nucleotides of the 3′ exon (E2), and the ribozyme contains all but the six 3′-terminal nucleotides of the intron (Figure 1B). After reaction to generate the E1/E2 product, the intron can catalyze a spliced exon reopening (SER) hydrolytic reaction that is mechanistically analogous to the reverse of the second step of splicing (Figure 1A; *25*). We previously demonstrated that both the exon ligation (E1/E2) and SER (E2) reaction products comigrate with independently synthesized standards and that splicing occurs only in the presence of ribozyme, E1, and divalent metal ions (*5*).

In the context of a bimolecular assay for the second step of splicing, in which E1 attacks the 3′ splice site of a linear intron/E2 construct, substitution of the terminal cytidine of E1 with 2′-deoxycytidine significantly slows the rate of exon ligation and appears to render the chemical step rate-limiting (*19*). For this reason, the E1 oligonucleotide used in our studies contained a 3′-terminal 2′-deoxycytidine residue (E1dC). Additionally, all of the reactions contained saturating concentrations of E1dC such that all of the ribozyme was present as the E·E1dC complex (E^{E1dC}). Scheme 2 summarizes the results of the kinetic investigation described here for the tripartite reaction.

The rate of exon ligation in the tripartite reaction as a function of ribozyme concentration (E^{E1dC}) in single turnover reactions with [S] ≪ K_M exhibits saturation behavior (Figure 2A). S_{WT} and E^{E1dC} react with an apparent second-order rate constant, $k_{cat}/K_M = 1.1 \times 10^4$ M^{-1} min^{-1}. The value of $K_M = 1.6$ μM most likely represents a true dissociation constant (see below) and indicates a relatively weak association between the substrate and E^{E1dC}. At high concentrations of

[1] Abbreviations: S, 3′ splice site oligonucleotide substrate, where the subscript WT denotes the unmodified ribose substrate and the other subscripts refer to cleavage site modifications; E, ribozyme; E^{E1dC}, ribozyme−exon 1 complex; $^{M}E^{E1dC}$, ribozyme−exon 1 complex with bound Mg^{2+} or Mn^{2+} as indicated; E^{E1dC}· S, ribozyme−exon 1 complex with bound substrate; $^{M}E^{E1dC}$· S, ribozyme−exon 1 complex with bound substrate and bound Mg^{2+} or Mn^{2+} as indicated; SER, spliced exon reopening; MOPS, 3-(*N*-morpholino)propanesulfonic acid; MES, 2-(*N*-morpholino)ethanesulfonic acid.

Scheme 2[a]

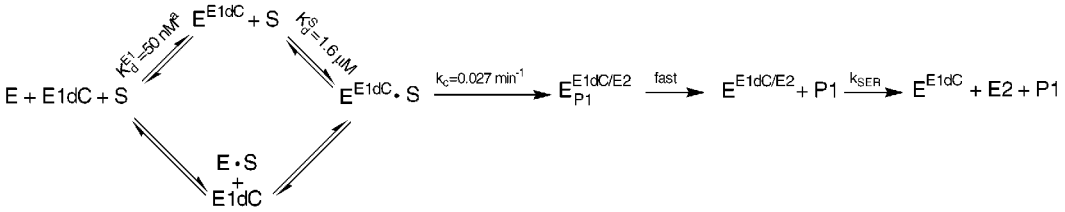

[a] This dissociation constant was estimated using an exon 1 oligonucleotide identical to E1dC except that the terminal C was ribose rather than deoxyribose (*61*). This 2′-hydroxyl group was previously shown to have only a 3-fold effect on binding (*58*).

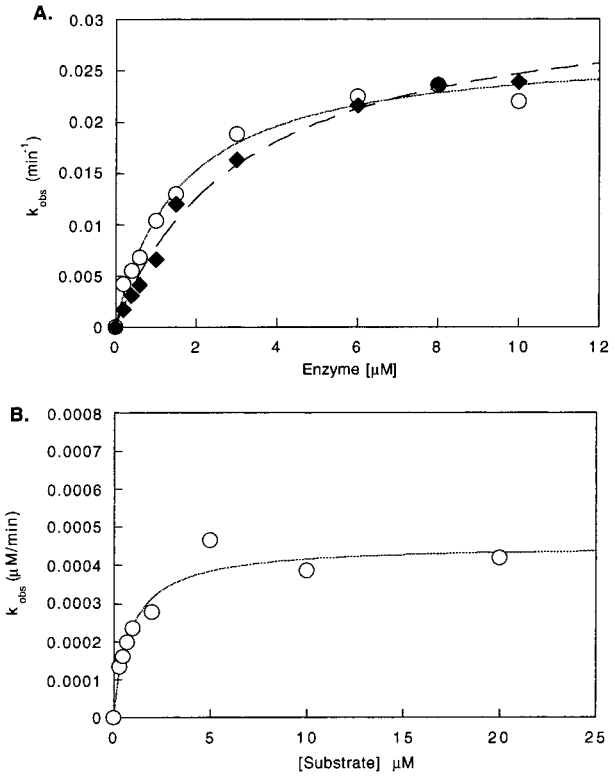

FIGURE 2: The tripartite assay obeys saturation kinetics under single and multiple turnover conditions. (A) Single turnover reactions contained 100 mM Mg^{2+} (circles) or 100 mM Mg^{2+}/10 mM Mn^{2+} (diamonds), ~1 nM 3′-radiolabeled substrate, and excess E^{E1dC} at the concentration indicated. The lines represent nonlinear least-squares fits of the data to a simple binding isotherm and give k_c and K_M values shown in Table 1. (B) Multiple turnover reactions contained 100 mM Mg^{2+}, 0.2 μM E^{E1dC}, ~1 nM radiolabeled substrate, and unlabeled substrate as specified. The line represents a nonlinear least-squares fit of the data according to the Michaelis−Menten equation and gives $V_{max} = 0.00045$ μM min^{-1} and $K_M = 0.8$ μM. The k_{cat} value was determined by dividing the maximum rate (V_{max}) obtained from the fit by the E^{E1dC} concentration.

E^{E1dC}, such that S_{WT} is fully bound, the observed rate (k_c) reflects the reaction of the ternary complex E^{E1dC}•S → [E^{E1dC}•S]‡. The k_c value determined from a nonlinear least-squares fit of the data gives $k_c = 0.027$ min^{-1}. Evidence presented below shows that the chemical step is rate-limiting for this reaction.

In multiple turnover experiments, we determined kinetic parameters by measuring the rate of product formation as a function of substrate concentration (Figure 2B). These experiments give a value of $K_M = 0.9$ μM, similar to that obtained under single turnover conditions. However, the value of $k_{cat} = 0.002$ min^{-1} is ~10-fold less than the value determined under single turnover conditions. As the single turnover reaction monitors the step that is rate-limiting up to the chemical cleavage step, the discrepancy in rates may arise either because product release is rate-limiting under multiple turnover conditions due to the tight binding of E1dC or because only a fraction of the enzyme is active. For these reasons, we conducted nearly all of our experiments under single turnover conditions.

For the second reaction step of *cis*-splicing, sulfur substitution of the *pro-R*$_P$, but not the *pro-S*$_P$, oxygen of the scissile phosphate strongly inhibits splicing (*8*). To confirm that the tripartite reaction reflects the authentic second step of splicing, we examined the phosphorothioate diastereoselectivity. The two diastereomers of the phosphorothioate substrate (Dharmacon Research) were separated by reverse-phase HPLC (Figure 3A; the R_P isomer eluted before the S_P isomer), and the stereochemical identity of each oligonucleotide was determined by nuclease P1 and snake venom phosphodiesterase digestion (*22*). We measured the rate of exon ligation for each diastereomer and a control substrate lacking sulfur substitution (Figure 3B). In single turnover reactions under k_{cat}/K_M conditions, the control substrate (S_{WT}) reacted to completion with $k_{obs} = 0.01$ min^{-1}. Both S_{S_P} (closed diamonds) and S_{R_P} (open triangles) reacted approximately 6-fold more slowly than S_{WT}, but with end points of 82% and 8%, respectively (Figure 3B). The observations that a low level of S_{R_P} spliced at the same rate as S_{S_P} and that S_{S_P} reacted to a slightly reduced end point relative to S_{WT} (82% vs 98%) are consistent with reciprocal contamination by each diastereomer. This is expected because the diastereomers lacked baseline separation during reverse-phase HPLC (despite extensive efforts to optimize the separation; Figure 3A) and contamination of the S_P diastereomer with the R_P diastereomer was evident from nuclease P1 digestion (data not shown). Thus, the tripartite reaction shares the same strong preference for the *pro-S*$_P$ isomer as *cis*-splicing, suggesting that exon ligation via the tripartite reaction occurs at the same active site used for exon ligation during canonical *cis*-splicing.

Evidence That the Chemical Step Is Rate-Determining in the Tripartite Reaction. Several independent approaches were used to investigate whether the chemical step of exon ligation is rate-limiting for the tripartite reaction. First, phosphorothioate substitution was used to probe the rate-limiting step (*26*, *27*). The observed 6-fold reduction in reaction rate of S_{S_P} relative to S_{WT} (Figure 3B) is similar to the effect of sulfur substitution in nonenzymatic nucleophilic substitution reactions of model phosphate diesters (4−11-fold; *26*). The observation that the "thio effect" on the reaction rate at the active site is the same as the intrinsic thio effect observed in model compounds suggests that chemistry is the rate-determining step for the tripartite reaction.

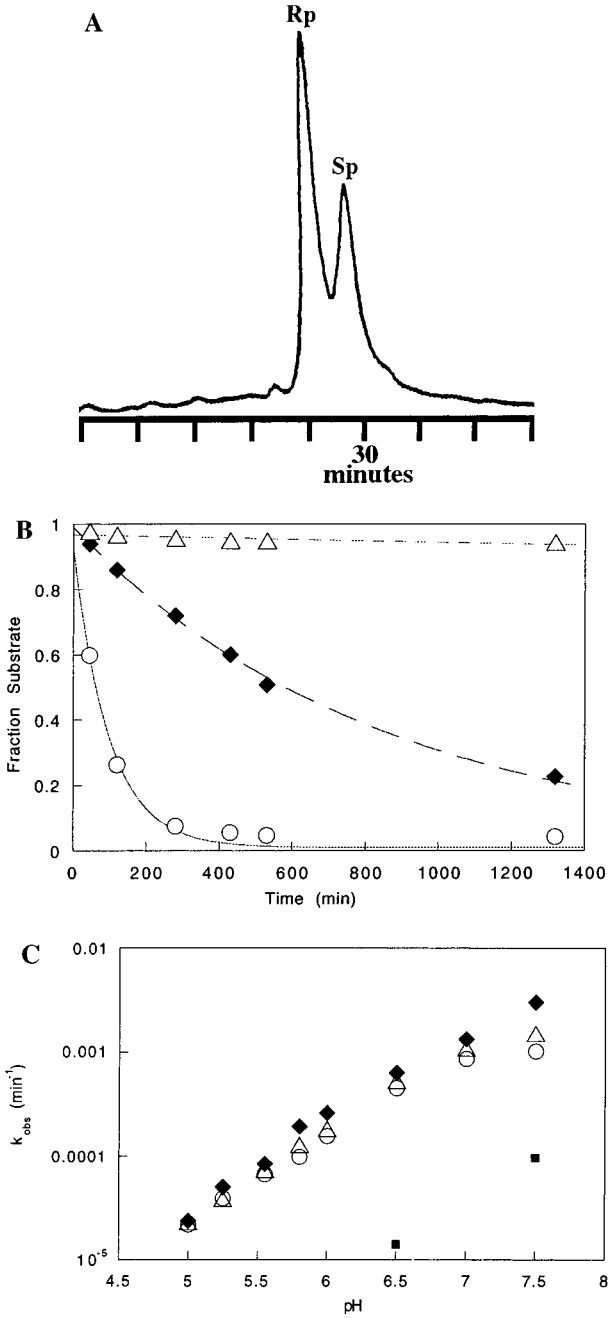

FIGURE 3: Evidence that the chemical step is rate-limiting in the tripartite reaction. (A) Reverse-phase HPLC chromatogram showing the separation of the R_P and S_P diastereomers of the 3′ splice site substrate containing a phosphorothioate at the cleavage site. (B) Time courses for single turnover reactions of the splicing of S_{WT} (circles), S_{S_P} (diamonds), and S_{R_P} (triangles) in 100 mM Mg^{2+}. Reaction end points for S_{WT}, S_{S_P}, and S_{R_P} were 98%, 82%, and 8%, respectively. The k_{obs} values were determined from an exponential fit to the data that accounted for the end points. (C) pH dependence of k_{obs} for S_{WT} in 100 mM Mg^{2+} (diamonds) and in 100 mM Mg^{2+}/10 mM Mn^{2+} (triangles) and for $S_{3'S}$ in 100 mM Mg^{2+} (squares) and in 100 mM Mg^{2+}/10 mM Mn^{2+}(circles). Linear fits to the data between pH 5.0 and pH 6.5 gave slopes of 1.04 (diamonds), 0.91 (triangles), and 0.83 (circles).

Second, we investigated the pH dependence of the tripartite reaction. In single turnover reactions in either 100 mM Mg^{2+} or 100 mM Mg^{2+}/10 mM Mn^{2+}, the rate of exon ligation in the reaction $E^{E1dC} + S \rightarrow [E^{E1dC}\cdot S]^{\ddagger}$ was log-linear with pH (Figure 3C), although the rate begins to plateau above pH 7.5 (data not shown). From pH 5.0 to pH 6.5, the slope for the pH dependence is ~1 (1.04 and 0.91 for Mg^{2+} and Mg^{2+}/Mn^{2+}, respectively). The same pH dependence was observed under conditions of saturating E^{E1dC} (see Figure 6A and text below), suggesting that the binding of S is independent of pH and indicating that a proton is lost from the $E^{E1dC}\cdot S$ ternary complex prior to the chemical cleavage step. Because the proton on the nucleophilic 3′-hydroxyl group of E1dC must be lost in the course of the reaction and its removal generates the more reactive 3′-oxyanion, the log-linear increase in rate with pH suggests that the tripartite reaction monitors the chemical step of exon ligation.

Third, if the tripartite reaction of S_{WT} monitors the chemical step, reaction of modified substrates that react significantly slower than S_{WT} should also monitor the chemical step and therefore show the same pH dependence as the reaction of S_{WT}. In 100 mM Mg^{2+}, a substrate in which the 3′-oxygen leaving group is substituted with sulfur ($S_{3'S}$) reacts ~100-fold slower than S_{WT}. However, both S_{WT} and $S_{3'S}$ reacted ~10-fold faster upon raising the pH from 6.5 to 7.5 (Figure 3C), suggesting that the reaction of $S_{3'S}$ follows the same pH dependence as S_{WT}. This observation implies that the reactions of $S_{3'S}$ and S_{WT} monitor the same step and further strengthens the argument that the chemical step is rate-limiting. Experiments below provide evidence that a second slower reacting substrate, in which the 2′-OH at the 3′ splice site is replaced by an amino group ($S_{2'N}$), also reacts with the same pH dependence as S_{WT} when Mg^{2+} is the only divalent metal ion (Figure 6A).

3′-Sulfur Substitution at the 3′ Splice Site Results in a Metal Specificity Switch. Divalent metal ions exhibit preferences in coordinating inner-sphere ligands (*28*, *29*). "Hard" metal ions, such as Mg^{2+}, exhibit low affinities for sulfur and nitrogen ligands, whereas "softer" metal ions, such as Mn^{2+}, Co^{2+}, Cd^{2+}, or Zn^{2+}, coordinate sulfur, nitrogen, and oxygen ligands. A switch in metal specificity upon substitution of sulfur or nitrogen for oxygen can be indicative of direct coordination between the metal ion and the substituted atom (*5*, *9*, *10*, *30*−*35*). Such analyses are especially powerful when the following two criteria are met: (1) the effect of the softer metal ions (M^{2+}) on the reactivity of both the "wild-type" and modified substrates is measured so that the rescue, defined as $[(k_{obs}{}^{S_{WT}}/k_{obs}{}^{S_{3'S}})^{Mg^{2+}}/(k_{obs}{}^{S_{WT}}/k_{obs}{}^{S_{3'S}})^{M^{2+}}]$, reflects the effect of the metal ion that is specific to the modification on S (*20*, *30*, *31*), and (2) the same elementary steps are monitored for both the wild-type and modified substrates (*20*, *31*).

We previously showed that sulfur substitution of the 3′-oxygen leaving group at the 3′ splice site had no significant effect on the rate of *cis*-splicing, even in the absence of thiophilic metal ions such as Mn^{2+} or Zn^{2+} (*5*). However, when the effect of this substitution was monitored in the tripartite reaction under k_{cat}/K_M conditions (subsaturating E^{E1dC}), the result was very different (*5*). In Mg^{2+} the rate of exon ligation was reduced ~100-fold, and this effect was rescued almost completely by the addition of thiophilic metal ions. We concluded that the group II intron uses a divalent metal ion to stabilize the leaving group in the second step of splicing. Because those experiments were carried out under k_{cat}/K_M conditions, we could not distinguish whether the thio effect or its rescue by Mn^{2+} arises from the binding of the substrate, the chemical step, or both.

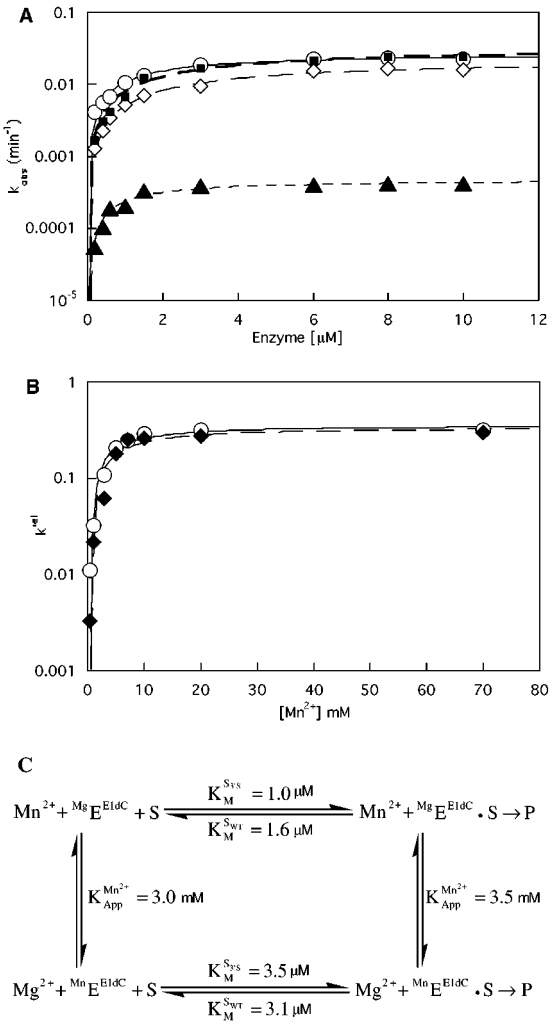

FIGURE 4: Mn^{2+} rescues the reactivity of $S_{3'S}$ relative to S_{WT}. (A) Dependence of k_{obs} for S_{WT} and $S_{3'S}$ on E^{E1dC} concentration. Reactions were single turnover in the presence of 100 mM Mg^{2+} (S_{WT}, circles; $S_{3'S}$, triangles) or 100 mM Mg^{2+}/10 mM Mn^{2+} (S_{WT}, squares; $S_{3'S}$, diamonds). The data in (B) show that Mn^{2+} is saturating in these assays. The lines are fits by nonlinear least squares to a simple binding isotherm and give k_c and K_M values shown in (C) and Table 1. (B) The effect of Mn^{2+} on the reactivity of $S_{3'S}$ and S_{WT} was determined under single turnover conditions with subsaturating (k_{cat}/K_M, diamonds) and saturating (k_c, circles) E^{E1dC}. To account for nonspecific effects of Mn^{2+}, the rate of $S_{3'S}$ is plotted relative to that of S_{WT} ($k^{rel} = k^{S3'S}/k^{SWT}$) at each Mn^{2+} concentration. Fits of the data to a binding isotherm for a single metal ion as previously described (*20*) gave the apparent dissociation constants shown in (C). (C) Thermodynamic cycle showing the relationship between the binding of substrate (S_{WT} and $S_{3'S}$) and rescuing metal ion to the ground-state E^{E1dC} complex. Metal ion and substrate dissociation constants were determined from the data in (A) and (B).

To distinguish these possibilities and extend our analyses, the Michaelis constants of $S_{3'S}$ and S_{WT} were determined in both 100 mM Mg^{2+} and 100 mM Mg^{2+}/10 mM Mn^{2+} by measuring the rate of product formation through a range of E^{E1dC} concentrations. It is qualitatively apparent from Figure 4A that the thio effect in Mg^{2+} and the rescue by Mn^{2+} are the same at all enzyme concentrations tested [i.e., under both k_{cat}/K_M (subsaturating E^{E1dC}) and k_c (saturating E^{E1dC}) conditions], indicating that the effects of sulfur substitution and rescue do not arise from differences in ground state binding between the modified and normal substrate. The data in Figure 4A were fit by nonlinear least-squares to a binding curve. S_{WT} and $S_{3'S}$ both have K_M values in the low micromolar range in Mg^{2+} and Mn^{2+}. Because the binding of the substrate is weak and the chemical step is rate-limiting, the K_M values are expected to equal true equilibrium constants (K_d) for the dissociation of S from the E^{E1dC}·S complex. Thus, the similar affinities of S_{WT} and $S_{3'S}$ in Mg^{2+} and Mn^{2+} suggest that the ribozyme and catalytic metal ion do not interact with the 3′ leaving group in the ground state E^{E1dC}·S complex.

Affinity of the Mn^{2+} That Rescues $S_{3'S}$. Addition of 10 mM Mn^{2+} specifically stimulates the reaction rate of $S_{3'S}$ to within 3−4-fold of the rate of S_{WT} (Figure 4B). The Mn^{2+} concentration dependence of this stimulation facilitates determination of the affinity of the rescuing metal ion, as described by Shan et al. (*38*). The effect of Mn^{2+} specific to $S_{3'S}$ was isolated by plotting the reactivity of $S_{3'S}$ relative to S_{WT} (k^{rel}, Figure 4B). Both under k_{cat}/K_M and k_c conditions, the Mn^{2+} concentration dependence of k^{rel} is consistent with the binding of a single Mn^{2+} that specifically stimulates the reaction of $S_{3'S}$ [$K_d^{Mn^{2+}} = 3.1$ mM (k_{cat}/K_M) and 3.5 mM (k_c), Figure 4A,B]. These are apparent dissociation constants because all reactions are performed in a background of 100 mM Mg^{2+}. Under k_{cat}/K_M conditions the substrate is not bound to the enzyme in the initial ground state, and the apparent dissociation constant of the rescuing metal ion reflects the "intrinsic" affinity of this metal ion for the E^{E1dC} complex (*20*). Under k_c conditions, the substrate is bound to the ribozyme in the initial ground state and could influence the binding of the metal ion. The similar affinities of the rescuing metal ion under both k_c and k_{cat}/K_M conditions show that the substrate does not influence binding of the catalytic metal ion, suggesting that the metal ion does not interact with the substrate in the starting ground state. The absence of an effect on the affinity of the Mn^{2+} from bound S is consistent with the observation that the affinity of $S_{3'S}$ is not affected by Mn^{2+}, according to the thermodynamic cycle of Figure 4C.

The Metal Specificity Switch Is Masked under Cis-Splicing Conditions. We previously argued that a conformational change limits the overall rate of *cis*-splicing because the 100-fold effect observed in the Mg^{2+}-assisted tripartite reaction upon 3′-sulfur substitution at the 3′ splice site did not occur during *cis*-splicing (*5*). To address whether a ∼100-fold reduction in the rate of the chemical step under *cis*-splicing conditions could be masked by a slower conformational change, we compared the rate of the hydrolytic pathway of *cis*-splicing (*24*) with the rate of exon ligation of $S_{3'S}$ in the tripartite reaction. Both reactions were at pH 7.5 and contained 100 mM Mg^{2+} and 0.5 M $(NH_4)_2SO_4$. The tripartite reaction was performed with excess E1rC and saturating ribozyme so that it was functionally similar to the hydrolytic pathway of *cis*-splicing (E^{E1rC}·S → P), with the exception of the nick between nucleotides 881/882 of the intron (Figure 1A,B). The rate of the tripartite reaction with $S_{3'S}$ was ∼3-fold faster than *cis*-splicing (Figure 5: 0.0013 vs 0.0043 min^{-1}), supporting the hypothesis that the metal specificity switch is masked under *cis*-splicing conditions.

The 2′-OH at the 3′ Splice Site Is Important for Exon Ligation. During the initial design phase of our metal specificity switch experiments, we tested whether the 2′-OH at the 3′ splice site was important in the tripartite

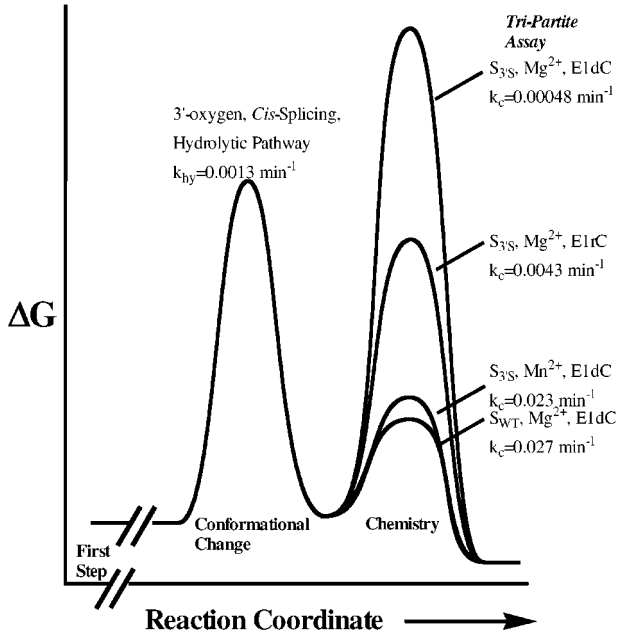

FIGURE 5: Free energy diagram showing why a metal specificity switch is observed in the tripartite reaction but not during the second step of *cis*-splicing. Even after sulfur substitution, the rate of reaction of the $E^{E1rC}\cdot S_{3'S}$ complex in Mg^{2+} is still faster ($k_c = 0.0043\ min^{-1}$) than the hydrolytic rate of *cis*-splicing ($k_{hyd} = 0.0013\ min^{-1}$). If the reactivity of the E1rC·E−E2 intermediate that occurs during hydrolytic splicing undergoes exon ligation at the same rate as that of the $E^{E1rC}\cdot S_{3'S}$ complex of the tripartite reaction, the deleterious effect of sulfur substitution on the exon ligation step would be completely masked, and no metal specificity switch would have been observed during *cis*-splicing. In contrast, the tripartite reaction with E1dC shows that sulfur substitution reduces the exon ligation rate of the $E^{E1dC}\cdot S_{3'S}$ complex by $\sim 10^2$-fold, but Mn^{2+} restores this activity to within 2-fold of the oxygen substrate ($E^{E1dC}\cdot S_{WT}$).

reaction. Efficient splicing of a substrate containing a 2′-deoxyuridine at the cleavage site would have allowed us to probe metal ion catalysis using 3′-thio-2′-deoxyuridine, rather than the synthetically less accessible 3′-thioribonucleoside. However, substitution of the 2′-OH at the cleavage site with a hydrogen atom reduced the rate of exon ligation ~700-fold relative to the ribose substrate (Table 1). This represents a loss of 4.1 kcal/mol of transition state stabilization. A priori, one or more of the following models can account for the contribution of the 2′-OH: (i) the 2′-OH accepts a hydrogen bond; (ii) the 2′-OH donates a hydrogen bond; (iii) the 2′-OH interacts with an active site divalent metal ion that is essential for catalysis. Each of these models was tested by combining atomic mutagenesis with quantitative analysis (Table 1).

Does the 2′-OH Accept a Hydrogen Bond? To investigate whether the 2′-OH at the cleavage site accepts a hydrogen bond that is important for catalysis, it was substituted with a fluorine atom (−F) or a methoxy ($-OCH_3$) group, both of which might accept but cannot donate a hydrogen bond. The reactivity of each substrate was determined with saturating E^{E1dC} in both 100 mM Mg^{2+} and 100 mM Mg^{2+}/10 mM Mn^{2+}. As the rate of reaction of $S_{2'F}$ with E1dC was too slow to measure accurately, the rate was determined with E1rC, which reacts ~40-fold faster than E1dC with S_{WT}. Table 1 shows that the 2′-F and 2′-OCH_3 substitutions significantly reduce the cleavage rate relative to S_{WT} and provide no substantial rate acceleration relative to a hydrogen atom. Additionally, the reaction rates for both substrates were stimulated less than 2-fold in the presence of Mn^{2+}. These results do not support the model that the ability to accept a hydrogen bond gives rise to the contribution of the 2′-OH in the transition state. Additionally, 2′-fluoronucleosides and ribonucleosides both favor the 3′-endo sugar conformation relative to 2′-deoxynucleosides (*36*). Thus, the poor reactivity of the $S_{2'F}$ suggests that the catalytic contribution of the 2′-OH cannot arise solely from its tendency (relative to 2′-H) to favor the 3′-endo sugar conformation.

Does the 2′-OH Donate a Hydrogen Bond? To test whether the 2′-OH donates a hydrogen bond during catalysis, we examined the reactivity of a substrate in which the 2′-OH at the cleavage site is substituted with an amino group ($S_{2'N}$). The pK_a of the 2′-amino group is expected to be ~6.1−6.2 (*37*, *38*). We first probed the reactivity of $S_{2'N}$ at pH 7.5 in the presence of saturating ribozyme and 100 mM Mg^{2+}. $S_{2'N}$ reacts ~50-fold slower than S_{WT} but, unlike $S_{2'F}$ and $S_{2'OCH_3}$, $S_{2'N}$ gives a rate enhancement of ~10-fold relative to $S_{2'H}$, suggesting that the ability to donate a hydrogen bond might be important for catalysis. To test this further, we measured the pH dependence of $S_{2'N}$ (Figure 6A). At low pH (<6.2) the amino group should be protonated ($-NH_3^+$) and can donate but not accept a hydrogen bond. Figure 6A shows that the pH dependence of $S_{2'N}$ parallels S_{WT} throughout the pH range and is log-linear from pH 5 to pH 6.5 (Figure 6A, compare triangles and filled circles). Thus, there is no additional rate acceleration gained from deprotonating the 2′-NH_3^+ group to free a lone pair of electrons.[2] Otherwise, the pH dependence of $S_{2'N}$ would be steeper than that for S_{WT}. These results show that in Mg^{2+} the reactivity of $S_{2'N}$ is not sensitive to the presence of the lone pair of electrons at the 2′ position and further argue against the model that the 2′-OH accepts a hydrogen bond during catalysis.

Precedence for hydrogen bond donation by a cleavage site 2′-OH exists in the literature. The 2′-OH at the cleavage site of the group I ribozyme facilitates the chemical step by donating a hydrogen bond to the neighboring 3′-oxygen leaving group in the transition state, presumably serving to stabilize the developing negative charge (*39*). We substituted the 3′-oxygen leaving group with sulfur to investigate whether the group II intron implements a similar catalytic strategy. As sulfur is a poor hydrogen bond acceptor (*39*), the catalytic contribution of the 2′-OH will be diminished when its hydrogen-bonding partner is substituted by sulfur. The reaction rates of $S_{3'S/2'H}$ and $S_{3'S/2'OH}$ were measured with saturating ribozyme in 100 mM Mg^{2+}/10 mM Mn^{2+} at pH 7.5. Mn^{2+} was included because the reactivity of the 3′-thio substrate in Mg^{2+} is severely inhibited. The rate constant for $S_{3'S/2'H}$ was reduced $\sim 10^3$-fold relative to $S_{3'S/2'OH}$ (Table 1). The observation that the 2′-OH significantly increases the reactivity of both the 3′-thio and 3′-oxygen substrates relative to their 2′-deoxy counterparts suggests that the 2′-OH does not facilitate catalysis by donating a hydrogen bond to the 3′-oxygen leaving group.

[2] This experiment does not rule out the possibility that the active site of the ribozyme shifts the pK_a of the amino group to an anomalous value such that it is either fully protonated or deprotonated throughout the pH range of the experiment. However, experiments below with Mn^{2+} suggest that the active site environment does not perturb the pK_a of the 2′-amino group relative to solution.

Table 1: The Effect of Cleavage Site Modifications on the Rate of Exon Ligation in the Tripartite Reaction[a]

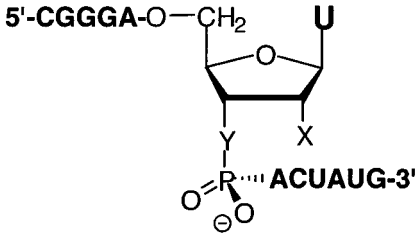

3' Splice Site Oligoribonucleotide

		$k_c \times 10^{-4}$ (min^{-1})[b]		K_d (μM)[c]		K_i (μM)[d]	
X	Y	Mg^{2+} [e]	Mg^{2+}/Mn^{2+} [f]	Mg^{2+} [e]	Mg^{2+}/Mn^{2+} [f]	Mg^{2+} [e]	Mg^{2+}/Mn^{2+} [f]
OH	O	270	320	1.6	3.1	0.8	1.0
OH	S	4.0	220	1.0	3.5		
H	O	0.36	0.45			1.6	
H	S		0.12				
F	O	~0.06 (2.4)[g]	~0.06 (2.6)[g]			2.7	
OCH_3	O	0.75	1.1			1.0	
NH_2	O	4.0	33	2.2	1.8	1.9	1.7

[a] Reactions were carried out at 42 °C with 0.5 M $(NH_4)_2SO_4$ and 40 mM MOPS (pH 7.5). [b] Reaction mixtures contained 9 μM E^{E1dC} or E^{E1rC}. [c] $[E^{E1dC}]$ was varied from 0 to 9−10 μM. [d] $[E^{E1dC}]$ was 0.2 μM. [e] $[Mg^{2+}] = 100$ mM. [f] $[Mg^{2+}] = 100$ mM, and $[Mn^{2+}] = 10$ mM. [g] Because the rate of $S_{2'F}$ with E^{E1dC} was too slow to measure accurately, this rate was determined with E^{E1rC}, which reacts with S_{WT} ~40-fold faster than E^{E1dC}.

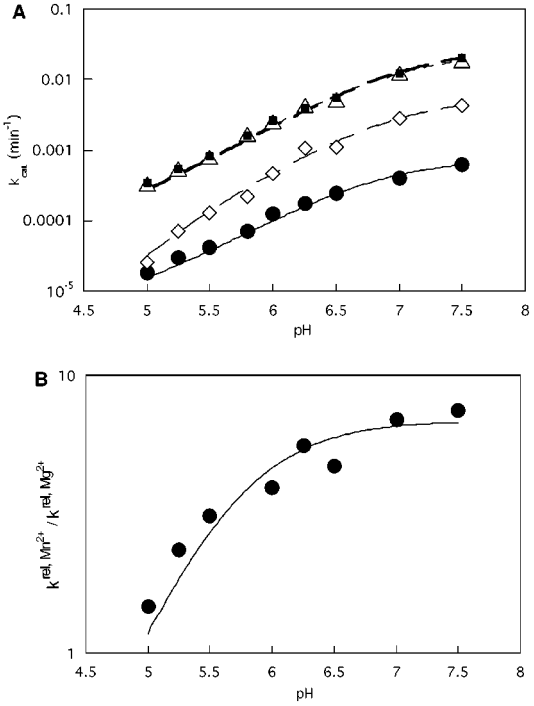

FIGURE 6: (A) pH dependence of k_c for S_{WT} and $S_{2'N}$ in 100 mM Mg^{2+} (S_{WT}, triangles; $S_{2'N}$, filled circles) and 100 mM Mg^{2+}/10 mM Mn^{2+} (S_{WT}, squares; $S_{2'N}$, diamonds). Reactions were single turnover with saturating E^{E1dC} (9 μM). Linear fits to the data between pH 5.0 and pH 6.25 gave slopes of 1.22 (diamonds), 0.78 (circles), and 0.84 (triangles, squares). (B) The pH dependence of the reactivity of $S_{2'N}$ in Mn^{2+} ($k^{rel,Mn^{2+}} = k^{Mn^{2+},S_{2'N}}/k^{Mn^{2+},S_{WT}}$) relative to the rate in Mg^{2+} ($k^{rel,Mg^{2+}} = k^{Mg^{2+},S_{2'N}}/k^{Mg^{2+},S_{WT}}$) is plotted using k_c values from (A). The cleavage rate of $S_{2'N}$ relative to S_{WT} in each metal is used rather than the observed rate to account for nonspecific effects of changing the pH. The data were fit to eq 1, which was derived from Scheme 1, and give the pK_a of the amino group of $E^{E1dC}\cdot S_{2'N}$ as 5.7−6.2.

Does the 2′-OH Interact with a Metal Ion? At low pH the amino group is protonated ($-NH_3^+$) and lacks a lone pair of electrons that can interact with a metal ion. However, when deprotonated ($-NH_2$) at higher pH, the lone pair of electrons on nitrogen can interact with softer metals such as Mn^{2+} more favorably than with Mg^{2+} (*29*, *34*). Thus, the pH dependencies for reactions of $S_{2'N}$ and S_{WT} were determined with saturating ribozyme in 100 mM Mg^{2+}/10 mM Mn^{2+} (Figure 6A, squares and diamonds). The reactivity of both substrates increases with pH, but Mn^{2+} specifically stimulates the rate of $S_{2'N}$. This rescue of $S_{2'N}$ increases with pH: at pH 5.0 and pH 7.5 the stimulation is 2-fold and 10-fold, respectively. As a result, between pH 5.0 and pH 6.5 the slope for $S_{2'N}$ in Mn^{2+} is significantly and reproducibly greater than the slope for $S_{2'N}$ in Mg^{2+} (Figure 6A; 1.22 vs 0.78). Presumably, the greater slope in Mn^{2+} reflects the additional deprotonation of the amino group to generate a lone pair of electrons on the nitrogen that can interact with the Mn^{2+}.[3] The different reactivities of the 2′-NH_2 and 2′-NH_3^+ groups in Mn^{2+} signal for the deprotonation of the amino group. A plot of $k^{rel,Mn^{2+}}/k^{rel,Mg^{2+}}$ (see Materials and Methods) gives a pK_a of 5.7−6.2 for the 2′-NH_3^+ group when bound to the ribozyme (Figure 6B). This pK_a value is similar to that observed for the 2′-NH_3^+ group in solution and suggests that the active site of the ribozyme does not perturb the pK_a of the amino group (*37*, *38*). This implies that the Mn^{2+} interaction with the amino group does not occur in the ground state $E^{E1dC}\cdot S$ complex. Additional support for this conclusion is provided below.

To investigate further the nature of the interaction between the metal ion and 2′-OH, dissociation constants for $S_{2'N}$ were determined in the absence (100 mM Mg^{2+}) and presence of Mn^{2+} (100 mM Mg^{2+}/10 mM Mn^{2+}) by measuring the rate of product formation over a range of ribozyme concentrations (Figure 7A). The data were fit according to a binding curve, and the dissociation constants determined at pH 5.5 and 7.5 are shown in the thermodynamic cycle in Figure 7C. The

[3] Apparently the 2′-NH_3^+ substrate has the same reactivity as the 2′-NH_2 substrate in Mg^{2+} even though the $-NH_3^+$ group contains no lone pair electrons to interact with Mg^{2+}. Two factors may allow the 2′-NH_3^+ group to compensate for the loss of the Mg^{2+}−nitrogen interaction: (1) the 2′-NH_3^+ group is more electron withdrawing than the 2′-NH_2 group and therefore may improve the leaving ability of the 3′-oxygen, and (2) the 2′-NH_3^+ is expected to be a better hydrogen bond donor than the 2′-NH_2 and therefore may provide greater transition state stabilization via hydrogen bond donation than the 2′-NH_2 does.

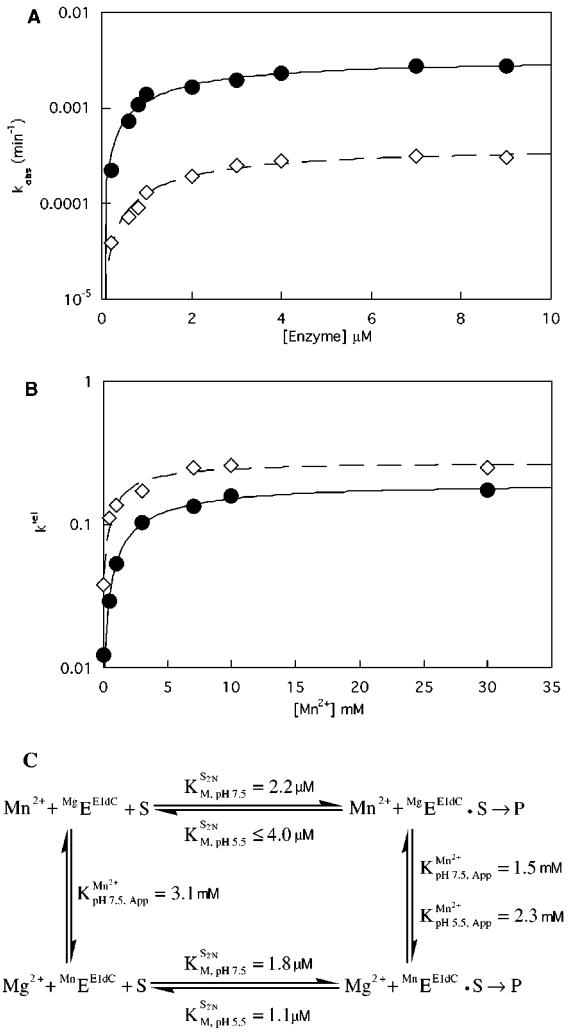

FIGURE 7: Thermodynamic analysis of the interaction between Mn^{2+} and the 2′-moiety of S. (A) The dissociation constants for $S_{2'N}$ were determined from the dependence of k_{obs} on E^{E1dC} concentration. Reactions were single turnover in the presence of 100 mM Mg^{2+} (diamonds) or 100 mM Mg^{2+}/10 mM Mn^{2+} (circles) at pH 7.5. The lines are fits by nonlinear least-squares to a simple binding isotherm and give k_c and K_M values shown in (C) and Table 1. (B) The effect of Mn^{2+} on the reactivity of S_{WT} and $S_{2'N}$ was determined under single turnover conditions with subsaturating (k_{cat}/K_M, circles) and saturating (k_c, diamonds) E^{E1dC} complex. The reaction with $S_{2'N}$ relative to S_{WT} ($k^{rel} = k^{S_{2'N}}/k^{S_{WT}}$) was determined at each Mn^{2+} concentration. The data were fit for a single metal ion binding as previously described (*20*), and the apparent dissociation constants are shown in (C). (C) Thermodynamic cycle showing the relationship between binding of the substrate (S_{WT} and $S_{2'N}$) and rescuing metal ion to the ground state E^{E1dC} complex. The cycle is incomplete at pH 5.5 because reactions were too slow to determine kinetic parameters. Metal ion and substrate dissociation constants were determined from the data in (A) and (B) and data not shown.

K_d determined at pH 5.5 in 100 mM Mg^{2+} represents an upper limit because below ~2 μM E^{E1dC} the cleavage rate cannot be measured accurately. Similar to S_{WT}, $S_{2'N}$ binds with low micromolar affinity (1.1−<4 μM) regardless of the presence of Mn^{2+} or the protonation state of the 2′-amino group. The observation that, within experimental error, binding of $S_{2'N}$ is not influenced by the addition of Mn^{2+} is consistent with the lack of an effect by Mn^{2+} on the pK_a of the amino group, further supporting the conclusion that the metal ion is not interacting with $S_{2'N}$ in the ground state (Figure 7A,C).

Affinity of the Mn^{2+} That Interacts with the 2′-Moiety of S. The Mn^{2+} concentration dependence of the rescue of $S_{2'N}$ was measured under both k_{cat}/K_M (pH 7.5) and k_c (pH 7.5, 5.5) conditions. The specific effect of Mn^{2+} on $S_{2'N}$ was determined by plotting the reactivity of $S_{2'N}$ relative to S_{WT} (Figure 7B, pH 7.5). At pH 7.5, the Mn^{2+} concentration dependence of k^{rel} is consistent with a single metal binding with an apparent dissociation constant of 3.1 mM (k_{cat}/K_M) and 1.5 mM (k_c) (Figure 7B). The dissociation constant of the Mn^{2+} in the presence of the bound substrate is within experimental error of that obtained in the absence of bound substrate and is consistent with a lack of energetic coupling between substrate and Mn^{2+} in the ground state, as already suggested by the lack of a Mn^{2+} effect on K_d for $S_{2'N}$ and by the lack of a pK_a shift of the 2′-amino group at the ribozyme active site. Consistent with this, within experimental error, similar dissociation constants were determined at pH 5.5 (Figure 7A) and under multiple turnover conditions at pH 7.5 (data not shown). The Mn^{2+} K_d determined under k_{cat}/K_M conditions reflects the affinity of the Mn^{2+} for the E^{E1dC} complex, as $S_{2'N}$ is not bound in the starting ground state. Because the Mn^{2+} affinity is not perturbed by modification of the substrate, this affinity can be compared to the affinity obtained for the Mn^{2+} that interacts with the 3′ leaving group. Identical affinities would be consistent with rescue by a single metal ion, whereas different affinities would suggest rescue by distinct metal ions. Our results show that the Mn^{2+} that rescues $S_{2'N}$ has the same affinity as the Mn^{2+} that rescues $S_{3'S}$ ($K_{d,Mn^{2+},app} \cong 3$ mM). The simplest model is that a single metal ion mediates interactions with the 2′- and 3′-oxygen atoms of the cleavage site ribose in the transition state.

Does the 2′-OH Influence Binding or Chemistry? Although the K_d values for $S_{2'N}$ compared to S_{WT} were similar and provided no indication that an interaction with the 2′-OH is important for the binding of S to the E^{E1dC} complex, we also examined binding of other 2′ analogues. The very slow reactions of $S_{2'H}$, $S_{2'F}$, and $S_{2'OCH_3}$ prevented us from determining K_d's from their cleavage rates versus ribozyme concentration. Instead, we probed the affinity of these analogues for the E^{E1dC} complex by measuring their ability to inhibit the splicing reaction of S_{WT}. Under k_{cat}/K_M conditions, the cleavage rate of S is proportional to the concentration of the free E^{E1dC} complex. Binding of a substrate analogue to E^{E1dC} will prevent the binding of S and inhibit the reaction. Because the reaction of E^{E1dC} and S is slow compared to the binding of the inhibitor, the K_i (determined from a plot of the observed cleavage rate of S_{WT} versus inhibitor concentration) should equal the equilibrium dissociation constant of the inhibitor from the E^{E1dC} complex. The K_d values for $S_{2'H}$, $S_{2'OCH_3}$, and $S_{2'F}$ were each in the low micromolar range and did not differ significantly from the K_d value for S_{WT}. These data provide further support that the stability of the ground-state E^{E1dC}·S complex is not affected by the identity of the 2′-moiety at the cleavage site and suggest the absence of an interaction between this position and the ribozyme in the ground state. Thus, the 2′-OH appears to make its 4.1kcal/mol contribution in the transition state exclusively.

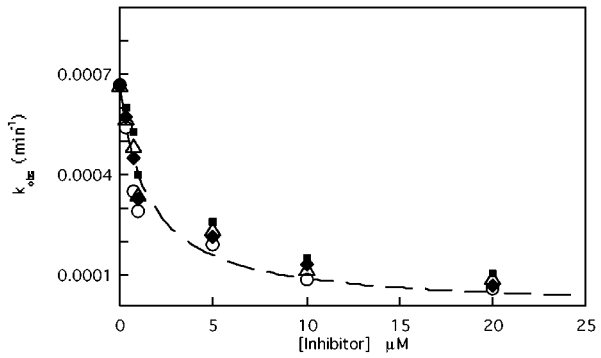

FIGURE 8: The substrates containing modifications at the 2′ position competitively inhibit the splicing of S_{WT}. Reactions were single turnover with trace radiolabeled S_{WT}, subsaturating E^{E1dC} (0.2 μM), and unlabeled $S_{2'OCH_3}$ (open circles), $S_{2'H}$ (diamonds), $S_{2'F}$ (closed squares), and $S_{2'NH_2}$ (triangles) inhibitor. The K_i values were determined from fits to the data and are shown in Table 1.

DISCUSSION

The Tripartite Reaction. The hydrolytic pathway of self-splicing by group II introns involves attack of exon 1 at the 3′ splice site of a linear intron−exon 2 intermediate (Figure 1A). If the intermediate is nicked just upstream of the 3′ splice site and the resulting two components, the intron (E) and a 3′ splice site oligonucleotide (S), are added separately to E1, a tripartite reaction occurs that mimics the second step of ai5γ group II intron self-splicing (Figure 1B). We have established a partial kinetic and thermodynamic framework summarized in Scheme 2. This framework allows dissection of the role of individual metal ions and functional groups in exon/splice site recognition and catalysis.

Several lines of evidence indicate that the chemical step is rate-limiting for the tripartite reaction when the nucleophile is E1dC. The reaction rate shows a log-linear dependence on pH with a slope of approximately unity between pH 5.0 and pH 6.5, both under k_c conditions and k_{cat}/K_M conditions, indicating that a proton is lost from the ternary E^{E1dC}•S complex prior to the rate-limiting step (Figure 3C). This pH dependence is expected for the chemistry of phosphoryl transfer because the 3′-hydroxyl group of E1dC loses a proton in the reaction and deprotonation prior to the chemical step would generate the more nucleophilic 3′-oxyanion. Consistent with the hypothesis that the chemical step is rate-limiting for the reaction of S, alternative substrates react with the same pH dependence as S even though they contain modifications that significantly slow the rate of reaction. For example, substitution of the 3′-oxygen leaving group with sulfur reduces the reaction rate in Mg^{2+} by ∼100-fold at pH 6.5, yet that substrate undergoes the same ∼10-fold increase in rate as S_{WT} when the pH is raised by one unit to 7.5 (Figure 3C). Substitution of the 2′-hydroxyl at the 3′ splice site with an amino group slows down the reaction rate in Mg^{2+} by ∼50-fold, yet that substrate shows the same pH dependence as S_{WT} throughout the entire pH range (Figure 6A). The observation that $S_{3'S}$ and $S_{2'N}$ react with the same pH dependence as S_{WT} suggests that the same step is rate-limiting for reaction of these substrates. However, if that step were a conformational step rather than the chemical step, then the observed rescue of reactivity of these substrates by Mn^{2+} would not be expected (see below). Finally, sulfur substitution of the *pro-S* oxygen at the scissile phosphate slows the rate of the reaction E^{E1dC}•S → $[E^{E1dC}$•S$]^{‡}$ by ∼6-fold (Figure 3B). This effect is similar in magnitude to the intrinsic effect of sulfur substitution in the nonenzymatic reactions of phosphate diesters with nucleophiles, further suggesting that the chemical step is rate-limiting (*26*).

The Cleavage Site 3′-Oxygen Interacts with a Metal Ion in the Transition State. We previously demonstrated that sulfur substitution of the 3′-oxygen leaving group shifts the metal specificity of the tripartite reaction from Mg^{2+} to Mn^{2+} (*5*). Although the observation of a metal specificity switch upon sulfur substitution in the tripartite reaction suggested that a metal ion stabilizes the leaving group in the second step of group II intron self-splicing, it was important to know what microscopic steps were being monitored in those experiments and whether the chemical step was rate-limiting. The partial kinetic framework developed herein shows that sulfur substitution of the 3′-oxygen leaving group has little effect on ground-state binding of S to the E^{E1dC} complex [$K_d(S_{3'S}) = 1.0$ μM, $K_d(S_{WT}) = 1.6$ μM] in Mg^{2+} but slows down the rate of the chemical step by ∼100-fold (Figure 4A). In the presence of Mn^{2+}, the binding of $S_{3'S}$ is again similar to the binding of S_{WT}, but the rate of cleavage of $S_{3'S}$ is significantly enhanced over that of S_{WT}. These results show that the effects of Mn^{2+} occur entirely in the chemical step and show that the affinity of the E^{E1dC} complex for S is sensitive neither to the identity of the 3′ leaving group atom nor to the identity of the metal ion. Thus, the thio effect and its rescue by Mn^{2+} are specific to the transition state, strongly supporting and extending our earlier proposal that the group II intron employs a metal ion to stabilize the leaving group in the second step of splicing (*5*). These results are in accordance with chemical considerations. The bridging oxygen of a phosphoester linkage is electropositive relative to the oxygen of a water molecule, and consequently, an interaction of the bridging oxygen with a divalent metal ion is unfavorable (*40*). However, a divalent metal ion could provide a stabilizing interaction in the transition state as charge accumulates on the 3′-oxyanion leaving group. Similar effects are documented for the group I intron (*30*, *41*).

Quantitative analysis of the reactivity of $S_{3'S}$ relative to S_{WT} as a function of Mn^{2+} concentration suggests that a single metal ion binds to rescue the 3′-thio substrate. The affinity measured under k_{cat}/K_M conditions ($K_{Mn^{2+},app} = 3.0$ mM) reflects the binding of the Mn^{2+} ion to the E^{E1dC} complex and is not affected by the modification on S because S is not bound in the starting ground state (Figure 4B). This thermodynamic fingerprint is a signature for the metal ion that interacts with the 3′-oxygen leaving group in the transition state of the second step of splicing and may be used to distinguish whether metal ion interactions with other ligands in the system are mediated by the same or by distinct metal ions (*20*; see below). Under k_c conditions, however, the affinity reflects the binding of the Mn^{2+} ion to the E^{E1dC}•S ternary complex and could be affected by S. The observation that Mn^{2+} binds with nearly the same affinity in the presence of bound S ($K_{Mn^{2+},app} = 3.5$ mM) as in its absence is further consistent with the aforementioned conclusion that the interaction between the Mn^{2+} and the leaving group occurs exclusively in the transition state.

In contrast to the results for sulfur substitution of the leaving group in the tripartite reaction, sulfur substitution at the 3′ splice site showed no effect on the rate of exon ligation during the *cis*-splicing reaction. To explain this apparent

discrepancy, we argued that a conformational change presumably limits the rate of formation of spliced exons rather than the actual chemical step (*5*). Here, we have gathered further evidence in support of this hypothesis by showing that the $E^{E1rC}\cdot S_{3'S}$ complex, which mimics the second step of *cis*-splicing for the sulfur-substituted precursor, produces ligated exons faster than the actual *cis*-splicing construct under the same conditions (Figure 5). Even the 100-fold effect of 3′-sulfur substitution is not large enough to render the chemical step rate-limiting during *cis*-splicing. Instead, a conformational step (*42*) that occurs after 5′ splice site cleavage masks the inhibitory effect of sulfur substitution and subsequent stimulatory effect by Mn^{2+} such that a metal specificity switch is not observed.

The Cleavage Site 2′-OH Interacts with a Metal Ion in the Transition State and May Donate a Hydrogen Bond. The 2′-OH at the 3′ splice site is essential for efficient catalysis as substitution of this 2′-OH with a hydrogen atom reduces the rate of reaction by 700-fold (Table 1). Like the metal ion interaction with the leaving group described above, the 2′-OH does not contribute to binding of S in the ground state [$K_d(S_{2'H}) = 1.6\ \mu M$, $K_d(S_{WT}) = 0.8\ \mu M$] but makes its contribution in the chemical step transition state. Modification of the substrate was used to investigate possible roles for the 2′-OH as a hydrogen bond acceptor, as a hydrogen bond donor, and/or as a ligand for a metal ion. Functional groups that potentially may accept a hydrogen bond, 2′-F and 2′-OCH_3, provide no rate enhancement relative to 2′-H. This may indicate that the 2′-OH at the 3′ splice site does not play a role as a hydrogen bond acceptor, but these results must be interpreted with caution for the following reasons. First, the ability of fluorine bonded to a sp^3-hybridized carbon to accept a hydrogen bond is questionable (*43*). Theoretical calculations estimate that the strength of a F···H hydrogen bond is only half as strong as an O···H hydrogen bond. Analysis of the organofluorine compounds deposited in the Cambridge Structural Database System revealed that short contacts between F and acidic hydrogens are surprisingly rare and occur with little angular dependence in the absence of additional geometrical constraints (*43*). Although these theoretical and statistical analyses imply that fluorine is a poor hydrogen bond acceptor, experimental analyses of protein and RNA interactions with ligands does provide support for F···H hydrogen bonds (*44*−*47*). Second, effects from 2′-OCH_3 substitution should also not be interpreted monolithically in terms of hydrogen-bonding capability as the hydrophobic nature of the methyl group could make contributions to the free energy of the interaction, and the steric bulk of the methyl group could occlude hydrogen bond formation completely. Despite these additional complications, however, the effect of 2′-OCH_3 substitution at the 3′ splice site in the tripartite reaction is similar to substitution by the smaller and less hydrophobic hydrogen atom, and this effect is again exerted exclusively in the transition state.

On the other hand, a 2′-amino substituent, which can donate a hydrogen bond, stimulates the cleavage rate k_c by ∼10-fold (pH 7.0, 100 mM Mg^{2+}) relative to 2′-H. Additionally, k_c for the reaction of $S_{2'N}$ exhibits the same pH dependence as S_{WT} (Figure 6A). Assuming that the active site environment does not dramatically perturb the pK_a of the amino group (see below), the similar pH dependence suggests that protonation of the 2′-NH_2 at the lower pH does not have a deleterious effect on the reaction. As the 2′-NH_3^+ group has lost its capacity to accept a hydrogen bond or coordinate to a metal ion, these results imply that $S_{2'N}$ reacts faster than $S_{2'H}$ in Mg^{2+} by virtue of its ability to donate a hydrogen bond.

Chemically and geometrically plausible hydrogen-bonding partners for the 2′-OH during the chemical step include the neighboring 3′-oxygen and the nonbridging oxygens of the reactive phosphoryl group, each of which may develop negative charge in the transition state. We tested the model in which the 2′-OH donates a hydrogen bond to the 3′-oxygen leaving group by examining the catalytic advantage of the 2′-OH in the context of a 3′-sulfur leaving group. In this model, the 2′-OH substituent would provide less transition state stabilization in the reaction of $S_{3'S}$ compared to the reaction of S_{WT} because sulfur is a weaker hydrogen bond acceptor than oxygen. This effect was observed previously in the *Tetrahymena* ribozyme reaction (*39*). In contrast, for the ai5γ ribozyme removal of the 2′-OH from $S_{3'S}$ reduced the rate of reaction of the ternary complex by $\sim 10^3$, similar to the effect on S_{WT} (Table 1), suggesting the absence of a hydrogen bond between the 3′-oxygen leaving group and the adjacent 2′-OH. The *pro*-R_P nonbridging oxygen is another potential hydrogen bond acceptor for the 2′-OH as sulfur substitution at this position inhibits exon ligation. However, we cannot test this model by determining the contribution of the 2′-OH to transition state stabilization because the reaction of the R_P-phosphorothioate is too slow to detect, even when the 2′-OH is present.

Finally, we tested whether the 2′-hydroxyl group acts as a ligand for an active site metal ion by probing the metal specificity of the reaction of $S_{2'N}$. Amino groups exhibit about a 10-fold preference in binding to Mn^{2+} relative to Mg^{2+} (*34*). Accordingly, in Mg^{2+} alone $S_{2'N}$ reacts about 50-fold slower than S_{WT} but is rescued ∼10-fold by the presence of Mn^{2+} (pH 7.0). The magnitude of this rescue decreased as the pH was lowered, suggesting that the rescue requires the unprotonated amino group. The specific rescue of $S_{2'N}$ therefore provides strong evidence for a direct interaction between Mn^{2+} and the 2′-nitrogen of S in the transition state of the second step of group II intron splicing. We infer an analogous interaction between Mg^{2+} and the 2′-OH of S at the ribozyme active site. The increase in reactivity of $S_{2'N}$ by Mn^{2+} provides a signal for binding of Mn^{2+} to E^{E1dC}. The apparent dissociation constant of this Mn^{2+} from the E^{E1dC} complex was obtained by quantitative analysis of the Mn^{2+} concentration dependence of $(k_{cat}/K_M)^{rel}$ [$=(k_c/K_M)^{Mn^{2+},S_{2'N}}/(k_c/K_M)^{Mn^{2+},S_{WT}}$]. This analysis suggests that a single Mn^{2+} binds to rescue the reaction of $S_{2'N}$. Because the substrate is not bound to the E^{E1dC} complex in the starting ground state under k_{cat}/K_M conditions, the binding of the Mn^{2+} is not affected by the modification on $S_{2'N}$. Thus, the affinity is intrinsic to the E^{E1dC} complex and may therefore be compared directly with the affinity of the metal ion that interacts with the 3′-oxygen leaving group. The affinity of the Mn^{2+} that interacts with the 2′ position of the cleavage site ribose ($K_d^{Mn^{2+}} = 3.1$ mM) is similar to the affinity of the Mn^{2+} that interacts with the 3′-oxygen leaving group ($K_d^{Mn^{2+}} =$ 3.0 mM). Although we cannot disprove a model in which two distinct metal ions bind with similar affinities, the simplest explanation is that a single divalent metal ion mediates both interactions. This model is geometrically

plausible, but the ribose hydroxyl groups are generally poor metal ion ligands (*48*, *49*), and the chelation of a single metal ion by neighboring 2′,3′-hydroxyl groups is relatively uncommon. Nevertheless, this kind of metal chelation has been observed in crystal structures of free nucleosides (*49*). Moreover, the interactions may become more favorable in the transition state if charge accumulates on one or both of the oxygen atoms.

The following evidence suggests that, similar to the interaction of the metal ion with the 3′-oxygen leaving group, the interaction of the metal ion with the 2′ position does not occur in the starting ground state. (1) The different reactivities of $S_{2'NH_3^+}$ and $S_{2'NH_2}$ in the reaction $E^{E1dC}\cdot S \rightarrow P$ in the presence of saturating Mn^{2+} (10 mM) provide a signal for deprotonation of the 2′-NH_3^+ group in the ternary complex. The value of p$K_{a,app}$, the negative logarithm of the observed equilibrium constant for deprotonation of $S_{2'NH_3^+}$ in the ternary complex, was obtained from the pH dependence of the rate of the chemical step with $S_{2'N}$ in the presence of Mn^{2+} relative to $S_{2'N}$ in Mg^{2+} alone. Fitting the pH dependence of k_c^{rel} to the model in Scheme 1 gives an apparent pK_a of 5.7−6.2 (Figure 6B). This value is not significantly different from the pK_a of the 2′-NH_3^+ group in solution (*37*, *38*). In contrast, a ground-state interaction of the metal ion with the 2′ position would be expected to shift the pK_a. (2) The apparent dissociation constant of the Mn^{2+} from the ternary complex $E^{E1dC}\cdot S$ was obtained by quantitative analysis of the Mn^{2+} concentration dependence of k_c^{rel} [$=k_c^{Mn^{2+},S_{2'N}}/k_c^{Mn^{2+},S_{WT}}$]. This analysis also shows that a single Mn^{2+} binds to rescue the reaction of the ternary complex. Because in these experiments substrate is bound to the E^{E1dC} in the starting ground state, the binding of Mn^{2+} could be affected by the modification on S. However, Mn^{2+} binds to the ternary complex with the same affinity ($K_d^{Mn^{2+}} = 1.5$ mM), within error, as it binds to the binary complex ($K_d^{Mn^{2+}} = 3.1$ mM), providing no evidence for thermodynamic coupling between the substrate and the metal ion in the ground state. (3) Analogously and consistent with the lack of an effect on Mn^{2+} binding by the presence of S, the presence of Mn^{2+} at the site that mediates the 2′ interaction in the transition state does not affect the affinity of $S_{2'N}$ for the ribozyme, as $S_{2'N}$ binds to the E^{E1dC} complex with the same affinity in the presence and absence of 10 mM Mn^{2+}.

This lack of ground-state interactions between the metal ion(s) and the ligands on S suggests that the $E^{E1dC}\cdot S$ ternary complex may be only partially folded or misfolded in the ground state such that S is not docked into the catalytic core of the ribozyme. To reach the catalytically active state, this "precatalytic" complex would have to undergo a conformational change to partially or fully align the catalytic groups and the reactants. The rate constant k_c for reaction of the ternary complex therefore may be a net rate constant that reflects the actual chemical step (k_c') and the equilibrium (K_{eq}) between this precatalytic complex and the catalytic complex. In support of this, the catalytic rate of a second-step reaction using a lariat 3′ exon ribozyme (*15*) is ~800-fold faster than the catalytic rate measured for the tripartite reaction (Figure 1), even though chemistry appears to be the rate-determining step in both reactions. This implies that the lariat structure directly influences the catalytic step, possibly by helping the RNA to maintain the conformation required for reaction. Accordingly, a genetically defined interaction

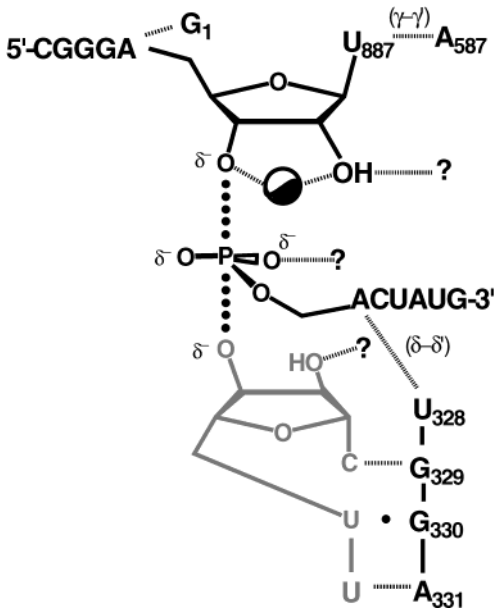

FIGURE 9: Model of the transition state for the second step of group II intron self-splicing. Interactions that position the 3′-hydroxyl nucleophile of exon 1 and the 3′ splice site are shown. The 3′-oxyanion leaving group and the cleavage site 2′-OH are metal ion ligands in the transition state. These interactions may be mediated by a single metal ion or by distinct metal ions that bind to the E^{E1dC} complex with the same affinity. The 2′-OH may also donate a hydrogen bond in the transition state. The strong deleterious effect of sulfur substitution of the *pro-R*$_P$ oxygen of the scissile phosphate suggests that it also participates in an interaction that facilitates catalysis. The interaction of the 2′-OH of E1 is inferred by the faster reaction rate of E^{E1rC} with S relative to that of E^{E1dC}. Other interactions between E and E1 and S are inferred from previous work (*18*, *50*, *53*). Adapted from Podar et al. (*19*).

between the first nucleotide of the intron (G1) and the penultimate nucleotide of the intron (A886) exists only when the second step of splicing occurs with the lariat/3′ exon intermediate and not with the linear intron/3′ exon intermediate (*50*). It was postulated that this interaction may influence the equilibrium between a correctly and incorrectly positioned 3′ splice site (*15*). A rapid equilibrium between catalytically competent and incompetent structures for the linear intron may result in a slower, but still chemically limited reaction (*15*). Alternatively, both the linear and lariat introns may form catalytically competent active sites, but a structural constraint imparted by the lariat that is absent in the linear form may provide an additional interaction that stabilizes the transition state. In the reactions catalyzed by the hammerhead ribozyme (*51*) and some mutant forms of the *Tetrahymena* ribozyme (*52*), some reorganization of the ground state is known to occur.

A Model for the Transition State of the Second Step of Splicing (Figure 9). Following the first step of splicing, the free 5′ exon remains bound to the intron by interacting with the exon binding sites (EBS1 and EBS2) in domain 1, which may help to align the 3′-OH nucleophile for attack at the 3′ splice site. Genetically defined δ/δ′ (*18*), γ/ γ′ (*50*), and nt 1/886 (*53*) interactions between the ribozyme and 3′ splice site region may help to position the 3′ splice site. The energetic contributions of these interactions to the ground state and the transition state are unknown. A divalent metal ion stabilizes the charge developing on the 3′-oxyanion leaving group in the transition state. The neighboring 2′-

OH contributes to transition state stabilization by interacting with the same, or possibly a distinct, metal ion and by donating a hydrogen bond. This interaction between the 2′-OH and the metal ion may help to bind and position the metal ion in the precatalytic complex so that it can stabilize the 3′-oxyanion leaving group in the transition state, and the metal ion may facilitate hydrogen bond donation by orienting the 2′-OH and lowering its pK_a. Ligands for this metal ion may be located in domain 5, which forms the core of the active site and has been implicated in metal ion binding (*54*−*56*). The *pro*-R_P oxygen of the reactive phosphoryl appears to form an essential interaction in the transition state. The nature of this interaction has yet to be defined. In contrast, the *pro*-S_P oxygen does not interact with the ribozyme in the transition state.

Interactions with the Ribose Phosphate at the Splice Sites: Comparison with Other RNA Splicing Systems. Metal ion specificity switch experiments have now established that metal ion stabilization of the leaving group is a strategy used for catalysis of both steps of splicing by three major splicing machineries—the self-splicing ai5γ group II intron from yeast (*5*), the spliceosome (*9*, *10*), and a self-splicing group I intron from *Tetrahymena thermophila* (*30*, *32*). The role of the cleavage site 2′-OH at the splice sites in each system has also been explored. Both the spliceosome and group II ribozyme exhibit similar asymmetric responses to 2′-deoxy substitution at the 5′ and 3′ splice sites—a modest effect at the 5′ splice site (*19*, *57*, *58*) and a strongly deleterious effect at the 3′ splice site (*57*; Table 1). We have shown here for the group II intron that the 2′-OH at the 3′ splice site coordinates to a metal ion and may donate a hydrogen bond. It will be interesting to determine whether the deleterious effect observed during nuclear pre-mRNA splicing occurs for the same reasons. For group I intron self-splicing by the *Tetrahymena* ribozyme, 2′-deoxy substitution at either splice site results in significant inhibition (*59*). The 2′-OH at the 5′ splice site is part of a hydrogen bond network and appears to donate a hydrogen bond to the neighboring 3′-hydroxyl leaving group, presumably acting together with a divalent metal ion to stabilize the developing negative charge in the transition state (*39*). As described here for the group II intron, the 2′-OH at the 3′ splice site of the group I intron also acts as a ligand for a metal ion (*33*, *34*). However, in contrast to our group II results, the metal that interacts with the 2′-OH ligand in the group I active site is clearly distinct from the metal ion that stabilizes the leaving group (*20*).

The lack of sequence or secondary structure similarity between group I and group II introns and the distinctive splicing pathways catalyzed by each suggest independent evolutionary origins for the two systems. Thus, the similarities in catalytic strategies that the two introns appear to share (at least qualitatively) might have arisen by convergent evolution for functional reasons or by accident from non-selected traits that were constrained from drifting during evolution. Either possibility may reflect an intrinsic limitation on the catalytic strategies available to RNA for catalysis of the phosphoryl-transfer reactions that occur during splicing (*60*). Before these issues can be resolved definitively, further work is necessary to address the mechanisms by which the nucleophiles are activated in each step of group II self-splicing and to uncover and elucidate additional active site features and their contributions to catalysis.

ACKNOWLEDGMENT

We thank Kelly Vereeke for excellent technical assistance and Cecilia Cortez for oligonucleotide synthesis. We are grateful to Melissa Moore and Avital Bar-Shalom for discussions and advice. We thank members of the Piccirilli laboratory for helpful discussions, advice, and comments on the manuscript.

REFERENCES

1. Michel, F., and Ferat, J.-L. (1995) *Annu. Rev. Biochem. 64*, 435−461.
2. Pyle, A. M. (1996) in *Catalytic RNA* (Ekstein, F., and Lilley, D. M. J., Eds.) pp 75−107, Springer-Verlag, Berlin, Germany.
3. Burge, C. B., Tuschl, T., and Sharp, P. A. (1999) in *The RNA World* (Gesteland, R. F., Cech T. R., and Atkins, J. F., Eds.) pp 525−560, Cold Spring Harbor Laboratory Press, Cold Spring Harbor, NY.
4. Nilsen, T. W. (1998) in *RNA structure and function* (Simons, R. W., and Grunberg-Manago, M., Eds.) pp 279−307, Cold Spring Harbor Laboratory Press, Cold Spring Harbor, NY.
5. Sontheimer, E. J., Gordon, P. M., and Piccirilli, J. A. (1999) *Genes Dev. 13*, 1729−1741.
6. Benner, S., and Ellington, A. D. (1988) *CRC Crit. Rev. Biochem. 23*, 369−426.
7. Moore, M. J., and Sharp, P. A. (1993) *Nature 365*, 364−368.
8. Padgett, R. A., Podar, M., Boulanger, S. C., and Perlman, P. S. (1994) *Science 266*, 1685−1688.
9. Sontheimer, E. J., Sun, S., and Piccirilli, J. A. (1997) *Nature 388*, 801−805.
10. Gordon, P. M., Sontheimer, E. J., and Piccirilli, J. A. (2000) *RNA 6*, 199−205.
11. Pyle, A. M., and Green, J. B. (1994) *Biochemistry 33*, 2716−2725.
12. Chin, K., and Pyle, A. M. (1995) *RNA 1*, 391−406.
13. Costa, M., and Michel, F. (1995) *EMBO J. 14*, 1276−1285.
14. Costa, M., Deme, E., Jacquier, A., and Michel, F. (1997) *J. Mol. Biol. 267*, 520−536.
15. Deme, E., Nolte, A., and Jacquier, A. (1999) *Biochemistry 38*, 3157−3167.
16. Jacquier, A., and Rosbash, M. (1986) *Science 243*, 1099−1104.
17. Jarrell, K. A., Peebles, C. L., Dietrich, R. C., Romiti, S. L., and Perlman, P. S. (1988) *J. Biol. Chem. 263*, 3432−3439.
18. Jacquier, A., and Jacquesson-Breuleux, N. (1991) *J. Mol. Biol. 219*, 415−428.
19. Podar, M., Perlman, P. S., and Padgett, R. A. (1998) *RNA 4*, 890−900.
20. Shan, S., Yoshida, A., Sun, S., Piccirilli, J. A., and Herschlag, D. (1999) *Proc. Natl. Acad. Sci. U.S.A. 96*, 12299−12304.
21. Sun, S., Yoshida, A., and Piccirilli, J. A. (1997) *RNA 3*, 1352−1363.
22. Slim, G., and Gait, M. J. (1991) *Nucleic Acids Res. 19*, 1183−1188.
23. Qin, P. Z., and Pyle, A. M. (1997) *Biochemistry 36*, 4718−4730.
24. Daniels, D. L., Michels, W. J., and Pyle, A. M. (1996) *J. Mol. Biol. 256*, 31−49.
25. Podar, M., Perlman, P. S., and Padgett, R. A. (1995) *Mol. Cell. Biol. 15*, 4466−4478.
26. Herschlag, D., Piccirilli, J. A., and Cech, T. R. (1991) *Biochemistry 30*, 4844−4854.
27. Michels, W. J., and Pyle, A. M. (1995) *Biochemistry 34*, 2965−2977.
28. Sigel, R. K. O., Song, B., and Sigel, H. (1997) *J. Am. Chem. Soc. 119*, 744−755.
29. Pearson, R. G. (1966) *Science 151*, 72−177.
30. Piccirilli, J. A., Vyle, J. S., Caruthers, M. H., and Cech, T. R. (1993) *Nature 361*, 85−88.
31. Curley, J. F., Joyce, C. M., and Piccirilli, J. A. (1997) *J. Am. Chem. Soc. 119*, 12691−12692.
32. Weinstein, L. B., Jones, B. C. N. M., Cosstick, R., and Cech, T. R. (1997) *Nature 388*, 805−808.

33. Sjogren, A. S., Pettersson, E., Sjoberg, B. M., and Stromberg, R. (1997) *Nucleic Acids Res. 25*, 648−654.
34. Shan, S., and Herschlag, D. (1999) *Biochemistry 38*, 10958−10975.
35. Basu, S., and Strobel, S. A. (1999) *RNA 5*, 1399−1407.
36. Saenger, W. (1983) in *Principles of Nucleic Acid Structure* (Cantor, C. R., Ed.) pp 51−101, Springer-Verlag, Berlin, Germany.
37. Aurup, H., Tuschl, T., Benseler, F., Ludwig, J., and Eckstein, F. (1994) *Nucleic Acids Res. 22*, 20−24.
38. Shan, S., Narlikar, G. J., and Herschlag, D. (1999) *Biochemistry 38*, 10976−10988.
39. Yoshida, A., Shan, S., Herschlag, D., and Piccirilli, J. A. (2000) *Chem. Biol. 7*, 85−96.
40. Bourne, N., and Williams, A. (1980) *J. Org. Chem. 49*, 1200−1204.
41. Narlikar, G. J., Gopalakrishnan, V., McConnell, T. S., Usman, N., and Herschlag, D. (1995) *Proc. Natl. Acad. Sci. U.S.A. 92*, 3668−3672.
42. Chanfreau, G., and Jacquier, A. (1996) *EMBO J. 15*, 3466−3476.
43. Howard, J. A. K., Hoy, V. J., O'Hagan, D., and Smith, G. T. (1996) *Tetrahedron 52*, 12613−12622.
44. Phelps, M. E., Hoffman, E. J., Sterlin, C., Huang, S. C., Robinson, G., McDonald, N., Schelbert, H., and Kuhl, D. E. (1978) *J. Nucl. Med. 19*, 1311.
45. Chapeau, M.-C., and Frey, P. A. (1994) *J. Org. Chem. 59*, 6994.
46. Bravo, P., Resnati, G., Angeli, P., Frigerio, M., Miani, F., Arone, A., Marucci, G., and Cantalamessa, F. (1992) *J. Med. Chem. 35*, 3102.
47. Pyle, A. M., Murphy, F. L., and Cech, T. R. (1992) *Nature 358*, 123−128.
48. Kazakov, S. A. (1996) in *Bioorganic Chemistry: Nucleic Acids* (Hecht, S. M., Ed.) pp 244−288, Oxford University Press, New York, NY.
49. Martin, R. B., and Mariam, Y. H. (1979) in *Metal Ions in Biological Systems* (Sigel, H., Ed.) Vol. 8, pp 57−114, Marcel Dekker, Inc., New York, NY.
50. Chanfreau, G., and Jacquier, A. (1993) *EMBO J. 12*, 5173−5180.
51. Mckay, D. B. (1996) *RNA 2*, 395−403.
52. Narlikar, G. J., Khosla, M., Usman, N., and Herschlag, D. (1997) *Biochemistry 36*, 2465−2477.
53. Jacquier, A., and Michel, F. (1990) *J. Mol. Biol. 213*, 437−447.
54. Peebles, C. L., Zhang, M., Perlman, P. S., and Franzen, J. S. (1995) *Proc. Natl. Acad. Sci. U.S.A. 92*, 4422−4426.
55. Abramovitz, D. L., Friedman, R. A., and Pyle, A. M. (1996) *Science 271*, 1410−1413.
56. Konforti, B. B., Abramovitz, D. L., Duarte, C. M., Karpeisky, A., Beigelman, L., and Pyle, A. M. (1998) *Mol. Cell 1*, 433−441.
57. Moore, M. J., and Sharp, P. A. (1992) *Science 256*, 992−997.
58. Griffin, E. A., Qin, Z., Michels, W. J., and Pyle, A. M. (1995) *Chem. Biol. 2*, 761−770.
59. Herschlag, D., Eckstein, F., and Cech, T. R. (1993) *Biochemistry 32*, 8312−8321.
60. Weiner, A. M. (1993) *Cell 72*, 161−164.
61. Bar-Shalom, A., and Moore, M. J. (2000) *Biochemistry* (in press).

BI001089O